

# MULTIPOLE ANALYSIS OF A BENCHMARK DATA SET FOR PION PHOTOPRODUCTION

R.A. ARNDT<sup>1</sup>, I. AZNAURYAN<sup>2</sup>, R.M. DAVIDSON<sup>3</sup>, D. DRECHSEL<sup>4</sup>,  
O. HANSTEIN<sup>4</sup>, S.S. KAMALOV<sup>5</sup>, A.S. OMELAENKO<sup>6</sup>, I. STRAKOVSKY<sup>1</sup>,  
L. TIATOR<sup>4</sup>, R.L. WORKMAN<sup>1</sup>, S.N. YANG<sup>7</sup>

<sup>1</sup> *Department of Physics, The George Washington University, Washington, D.C. 20052, U.S.A*

<sup>2</sup> *Yerevan Physics Institute, Alikhanian Brothers St. 2, Yerevan, 375036 Armenia*

<sup>3</sup> *Department of Physics, Applied Physics and Astronomy, Rensselaer Polytechnic Institute, Troy, NY 12180, U.S.A*

<sup>4</sup> *Institut für Kernphysik, Universität Mainz, 55099 Mainz, Germany*

<sup>5</sup> *Laboratory of Theoretical Physics, JINR, 141980 Dubna, Russia*

<sup>6</sup> *National Science Center, Kharkov Institute of Physics and Technology, Akademicheskaya St., 1, Kharkov, 61108, Ukraine*

<sup>7</sup> *Department of Physics, National Taiwan University, Taipei, Taiwan*

We have fitted low- and medium-energy benchmark datasets employing methods used in the MAID/SAID and dynamical model analyses. Independent fits from the Mainz, RPI, Yerevan, and Kharkov groups have also been performed over the low-energy region. Results for the multipole amplitudes are compared in order to gauge the model-dependence of such fits, given identical data and a single method for error handling.

## 1 Overview

The following report summarizes results from a series of fits to selected datasets for pion photoproduction, a project initiated by the Partial-Wave Analysis Working Group of BRAG (the Baryon Resonance Analysis Group). The goal of this work was an evaluation of the model-dependence inherent in multipole analyses of photoproduction data. In the past, groups have constructed their own databases, and the resulting differences have been shown to significantly effect some multipoles, in particular the E2/M1 ratio for the  $\Delta(1232)$ . The handling of systematic errors has also differed, the common choices being to either ignore them entirely, to combine them in quadrature with statistical errors, or to use them in ‘floating’ the angular distributions.

The construction of low-energy (180-450 MeV) and medium-energy (180-1200 MeV) datasets was carried out mainly for practical reasons. Many groups have studied the region below 450 MeV, which is dominated by the  $\Delta(1232)$ . Only a few groups have extended their analyses over the full resonance region. As the recent MAID and dynamical model fits (see the first contribution)

extend to 1 GeV, an upper limit of 1.2 GeV was chosen to include as many independent fits as possible.

The fitted data are listed on the BRAG website<sup>1</sup> and include differential cross section, target asymmetry ( $T$ ), and photon asymmetry ( $\Sigma$ ) data from proton targets only. The low- and medium-energy datasets were constructed to contain mainly recent measurements, with the goal of minimizing redundancies and simplifying the fitting procedure. In order to further simplify the exercise, systematic errors were not included in the fits. This should be kept in mind when  $\chi^2$  values are quoted.

Below we have compiled the reports of individual groups, giving details of the methods used, comments on the fit quality, and ways these results could be interpreted. Finally, in the last section, we summarize the findings of this study and suggest ways it could be improved or extended.

## 2 Multipole Analysis with MAID and a Dynamical Model

[ S.S. Kamalov, D. Drechsel, L. Tiator, and S.N. Yang ]

During the last few years we have developed and extended two models for the analysis of pion photo and electroproduction, the Dynamical Model<sup>2</sup> (hereafter called Dubna-Mainz-Taipei (DMT) model) and the Unitary Isobar Model<sup>3</sup> (hereafter called MAID). The final aim of such an analysis is to shed more light on the dynamics involved in nucleon resonance excitations and to extract  $N^*$  resonance properties in an unambiguous way. For this purpose as a testing ground we will use benchmark data bases recently created and distributed among different theoretical groups.

The crucial point in a study of  $N^*$  resonance properties is the separation of the total amplitude (in partial channel  $\alpha = \{l, j\}$ )

$$t_{\gamma\pi}^{\alpha} = t_{\gamma\pi}^{B,\alpha} + t_{\gamma\pi}^{R,\alpha} \quad (1)$$

in background  $t_{\gamma\pi}^{B,\alpha}$  and resonance  $t_{\gamma\pi}^{R,\alpha}$  contributions. In different theoretical approaches this procedure is different, and consequently this could lead to different treatment of the dynamics of  $N^*$  resonance excitation. As an example we will consider the two different models: DMT and MAID.

In accordance with Ref.<sup>2</sup>, in the DMT model the  $t_{\gamma\pi}^{B,\alpha}$  amplitude is defined as

$$t_{\gamma\pi}^{B,\alpha}(DMT) = e^{i\delta_{\alpha}} \cos \delta_{\alpha} \left[ v_{\gamma\pi}^{B,\alpha} + P \int_0^{\infty} dq' \frac{q'^2 R_{\pi N}^{(\alpha)}(q_E, q') v_{\gamma\pi}^{B,\alpha}(q')}{E - E_{\pi N}(q')} \right], \quad (2)$$

where  $\delta_\alpha(q_E)$  and  $R_{\pi N}^{(\alpha)}$  are the  $\pi N$  scattering phase shift and full  $\pi N$  scattering reaction matrix, in channel  $\alpha$ , respectively,  $q_E$  is the pion on-shell momentum. The pion photoproduction potential  $v_{\gamma\pi}^{B,\alpha}$  is constructed in the same way as in Ref.<sup>3</sup> and contains contributions from the Born terms with an energy dependent mixing of pseudovector-pseudoscalar (PV-PS)  $\pi NN$  coupling and t-channel vector meson exchanges. In the DMT model  $v_{\gamma\pi}^{B,\alpha}$  depends on 7 parameters: The PV-PS mixing parameter  $\Lambda_m$  (see Eq.(12) of Ref.<sup>3</sup>), 4 coupling constants and 2 cut-off parameters for the vector mesons exchange contributions.

In the extended version of MAID, the  $s$ ,  $p$ ,  $d$  and  $f$  waves of the background amplitudes  $t_{\gamma\pi}^{B,\alpha}$  are defined in accordance with the K-matrix approximation

$$t_{\gamma\pi}^{B,\alpha}(\text{MAID}) = \exp(i\delta_\alpha) \cos \delta_\alpha v_{\gamma\pi}^{B,\alpha}(q, W, Q^2), \quad (3)$$

where  $W \equiv E$  is the total  $\pi N$  c.m. energy and  $Q^2 = -k^2 > 0$  is the square of the virtual photon 4-momentum. Note that in actual calculations, in order to take account of inelastic effects, the factor  $\exp(i\delta_\alpha) \cos \delta_\alpha$  in Eqs.(2-3) is replaced by  $\frac{1}{2}[\eta_\alpha \exp(2i\delta_\alpha) + 1]$ , where both the  $\pi N$  phase shifts  $\delta_\alpha$  and inelasticity parameters  $\eta_\alpha$  are taken from the analysis of the SAID group<sup>4</sup>.

From Eqs. (2) and (3), one finds that the difference between the background terms of MAID and of the DMT model is that pion off-shell rescattering contributions (principal value integral) are not included in the background of MAID. From our previous studies of the  $p$ -wave multipoles in the (3,3) channel<sup>2</sup> it follows that they are effectively included in the resonance sector leading to the dressing of the  $\gamma N \Delta$  vertex. However, in the case of  $s$  waves the DMT results show that off-shell rescattering contributions are very important for the  $E_{0+}$  multipole in the  $\pi^0 p$  channel. In this case they have to be taken into account explicitly. Therefore, in the extended version of MAID we have introduced a new phenomenological term in order to improve the description of the  $\pi^0$  photoproduction at low energies,

$$E_{corr}(\text{MAID}) = \frac{\Delta E}{(1 + B^2 q_E^2)^2} F_D(Q^2), \quad (4)$$

where  $F_D$  is the standard nucleon dipole form factor,  $B = 0.71$  fm and  $\Delta E$  is a free parameter which can be fixed by fitting the low energy  $\pi^0$  photoproduction data. Thus the background contribution in MAID finally depends on 8 parameters. Below  $\pi^+ n$  threshold for both models we also take into account the cusp effect due to unitarity, as it was described in Ref.<sup>5</sup>, i.e.

$$E_{cusp} = -a_{\pi N} \omega_c \text{Re} E_{0+}^{\gamma\pi^+} \sqrt{1 - \frac{\omega^2}{\omega_c^2}}, \quad (5)$$

where  $\omega$  and  $\omega_c = 140$  MeV are the  $\pi^+$  c.m. energies corresponding to  $W = E_p + E_\gamma$  and  $W_c = m_n + m_{\pi^+}$ , respectively, and  $a_{\pi N} = 0.124/m_{\pi^+}$  is the pion charge exchange amplitude.

For the resonance contributions, following Ref.<sup>3</sup>, in both models the Breit-Wigner form is assumed, i.e.

$$t_{\gamma\pi}^{R,\alpha}(W, Q^2) = \bar{\mathcal{A}}_\alpha^R(Q^2) \frac{f_{\gamma R}(W)\Gamma_R M_R f_{\pi R}(W)}{M_R^2 - W^2 - iM_R\Gamma_R} e^{i\phi_R}, \quad (6)$$

where  $f_{\pi R}$  is the usual Breit-Wigner factor describing the decay of a resonance  $R$  with total width  $\Gamma_R(W)$  and physical mass  $M_R$ . The phase  $\phi_R(W)$  in Eq. (6) is introduced to adjust the phase of the total multipole to equal the corresponding  $\pi N$  phase shift  $\delta_\alpha$ .

The main subject of our study in the resonance sector is the determination of the strengths of the electromagnetic transitions described by the amplitudes  $\bar{\mathcal{A}}_\alpha^R(Q^2)$ . In general, they are considered as free parameters which have to be extracted from the analysis of the experimental data. In our two models we have included contributions from the 8 most important resonances, listed in the Table 1. The total number of  $\bar{\mathcal{A}}_\alpha^R$  amplitudes is 12 and they can be expressed also in terms of the 12 standard helicity elements  $A_{1/2}$  and  $A_{3/2}$ . Thus, to analyze experimental data we have a total of 19 parameters in DMT and 20 parameters in MAID. The final results obtained after the fitting of the high-energy (HE) benchmark data base with 3270 data points in the photon energy range  $180 < E_\gamma < 1200$  MeV are given in Table 1.

For the analysis of the low-energy (LE) data base with 1287 data points in the photon energy range  $180 < E_\gamma < 450$  MeV in the DMT model we used only 4 parameters: The PV-PS mixing parameter and 3 parameters for the  $P_{33}(1232)$  and  $P_{11}(1440)$  resonances. In MAID we have one more parameter due to the low energy correction given by Eq. (4). The final results for the helicity elements and the E2/M1 ratio (REM) are given in Table 2. In Table 3 we summarize our results and show the  $\chi^2$  obtained for different channels and different observables after fitting the LE and HE data bases. Note that the largest  $\chi^2$  in the LE fit we get for differential cross sections and target asymmetries in  $p(\gamma, \pi^0)p$ . Similar results were obtained practically in all other analyses. A detailed comparison with the results of different theoretical groups is given on the website <http://gwdac.phys.gwu.edu/analysis/pr.benchmark.html>. Below, in Fig. 1 we show only one interesting example, the  $E_{0+}$  multipole in the channel with total isospin 1/2. In this channel contributions from the  $S_{11}(1535)$  and  $S_{11}(1620)$  resonances are very important. At  $E_\gamma > 750$  MeV our values for the real part of the  ${}_pE_{0+}^{1/2}$  amplitude are mostly negative and lower than the

$N^*$		MAID current	MAID HE fit	DMT HE fit	PDG2000
$P_{33}(1232)$	$A_{1/2}$	-138	-143	—	$-135 \pm 6$
	$A_{3/2}$	-256	-264	—	$-255 \pm 8$
$P_{11}(1440)$	$A_{1/2}$	-71	-81	-77	$-65 \pm 4$
$D_{13}(1520)$	$A_{1/2}$	-17	-6	-7	$-24 \pm 9$
	$A_{3/2}$	164	160	165	$166 \pm 5$
$S_{11}(1535)$	$A_{1/2}$	67	81	102	$90 \pm 30$
$S_{31}(1620)$	$A_{1/2}$	0	86	37	$27 \pm 11$
$S_{11}(1650)$	$A_{1/2}$	39	32	34	$53 \pm 16$
$F_{15}(1680)$	$A_{1/2}$	-10	5	10	$-15 \pm 6$
	$A_{3/2}$	138	137	132	$133 \pm 12$
$D_{33}(1700)$	$A_{1/2}$	86	119	107	$104 \pm 15$
	$A_{3/2}$	85	82	74	$85 \pm 22$
PV-PS mixing:	$\Lambda_m$	450	406	302	
	$\Delta E$	2.01	1.73	—	
	$\chi^2/\text{d.o.f.}$	11.5	6.10	6.10	

Table 1. Proton helicity amplitudes (in  $10^{-3} \text{ GeV}^{-1/2}$ ), values of the PV-PS mixing parameter  $\Lambda_m$  (in MeV) and low-energy correction parameter  $\Delta E$  (in  $10^{-3}/m_{\pi^+}$ ) obtained after the high-energy (HE) fit

$N^*$		MAID current	MAID LE fit	DMT LE fit	PDG2000
$P_{33}(1232)$	$A_{1/2}$	-138	-142	—	$-135 \pm 6$
	$A_{3/2}$	-256	-265	—	$-255 \pm 8$
$P_{11}(1440)$	$A_{1/2}$	-71	-81	-93	$-65 \pm 4$
	REM(%)	-2.2	-1.9	-2.1	$-2.5 \pm 0.5$
	$\chi^2/\text{d.o.f.}$	4.76	4.56	3.59	

Table 2. Proton helicity elements (in  $10^{-3} \text{ GeV}^{-1/2}$ ) and REM=E2/M1 ratio (in %) obtained from the LE fit.

results of the SAID multipole analysis. The only possibility to remove such a discrepancy in our two models would be to introduce a third  $S_{11}$  resonance. Another interesting result is related to the imaginary part of the  ${}_pE_{0+}^{1/2}$  amplitude and, consequently, to the value of the helicity elements given in Table 1. Within the DMT model for the  $S_{11}(1535)$  we obtain  $A_{1/2} = 102$  for a total

Observables	LE			HE		
	N	MAID	DMT	N	MAID	DMT
$\frac{d\sigma}{d\Omega}(\gamma, \pi^+)$	317	4.68	3.32	871	6.36	5.95
$\frac{d\sigma}{d\Omega}(\gamma, \pi^0)$	354	7.22	5.74	859	6.87	5.85
$\Sigma(\gamma, \pi^+)$	245	2.79	2.57	546	4.57	6.49
$\Sigma(\gamma, \pi^0)$	192	2.22	1.58	488	7.65	7.65
$T(\gamma, \pi^+)$	107	3.28	2.94	265	3.75	4.17
$T(\gamma, \pi^0)$	72	5.18	4.84	241	5.31	5.65
Total	1287	4.56	3.64	3270	6.10	6.10

Table 3.  $\chi^2/N$  for the cross sections ( $\frac{d\sigma}{d\Omega}$ ), photon ( $\Sigma$ ) and target ( $T$ ) asymmetries in  $(\gamma, \pi^+)$  and  $(\gamma, \pi^0)$  channels obtained after LE and HE fit.  $N$  is the number of data points

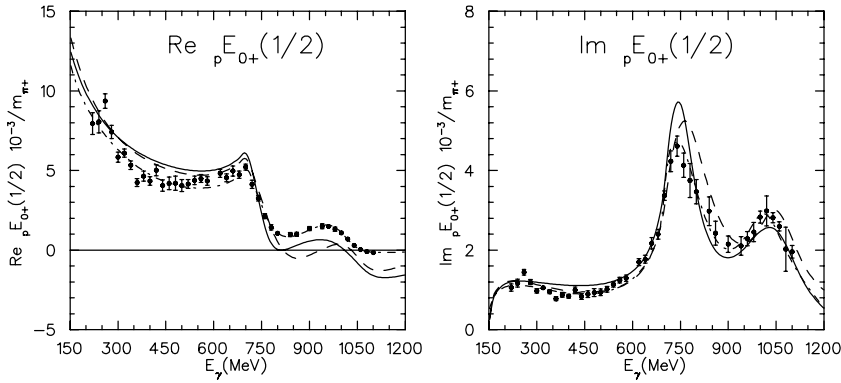


Figure 1.  $pE_{0+}^{1/2}$  multipole obtained after the HE fit using MAID (solid curves) and DMT (dashed curves). The dash-dotted curves and data points are the results of the global and single-energy fits obtained by the SAID group.

width of 120 MeV, which is more consistent with the results obtained in  $\eta$  photoproduction, than with previous pion photoproduction results obtained by the SAID and MAID groups.

### 3 Multipole Analysis of Pion Photoproduction with Constraints from Fixed- $t$ Dispersion Relations and Unitarity

[ O. Hanstein, D. Drechsel and L. Tiator ]

### 3.1 Outline of the Analysis

The method presented in Ref. <sup>6</sup> has been used to analyze the benchmark data set.

The starting point of our analysis is the fixed- $t$  dispersion relation for the invariant amplitudes<sup>7</sup>,

$$\text{Re}A_k^I(s, t) = A_k^{I,\text{pole}}(s, t) + \frac{1}{\pi} \mathcal{P} \int_{s_{\text{thr}}}^{\infty} ds' \left( \frac{1}{s' - s} + \frac{\varepsilon^I \xi_k}{s' - u} \right) \text{Im}A_k^I(s', t), \quad (7)$$

with the Mandelstam variables  $s$ ,  $u$  and  $t$ , the isospin index  $I = 0, \pm$ ,  $s_{\text{thr}} = (m_N + m_\pi)^2$ ,  $\varepsilon^I = \pm 1$  and  $\xi_k = \pm 1$ . The pole terms  $A_k^{I,\text{pole}}(s, t)$  are obtained by evaluating the Born approximation in pseudoscalar coupling.

The multipole projection of the dispersion relations (7) leads to a system of coupled integral equations of the form

$$\text{Re}\mathcal{M}_l^I(W) = \mathcal{M}_l^{I,\text{pole}}(W) + \frac{1}{\pi} \mathcal{P} \int_{W_{\text{thr}}}^{\infty} dW' \sum_{l'=0}^{\infty} \mathcal{K}_{ll'}^I(W, W') \text{Im}\mathcal{M}_{l'}^I(W'), \quad (8)$$

where  $\mathcal{M}_l^I(W)$  denotes any of the multipoles  $E_{l\pm}^I$  or  $M_{l\pm}^I$ . The integral kernels  $\mathcal{K}_{ll'}^I(W, W')$  are regular kinematical functions except for the diagonal kernels  $\mathcal{K}_{ll}^I$ , which contain a term  $\propto 1/(W - W')$ .

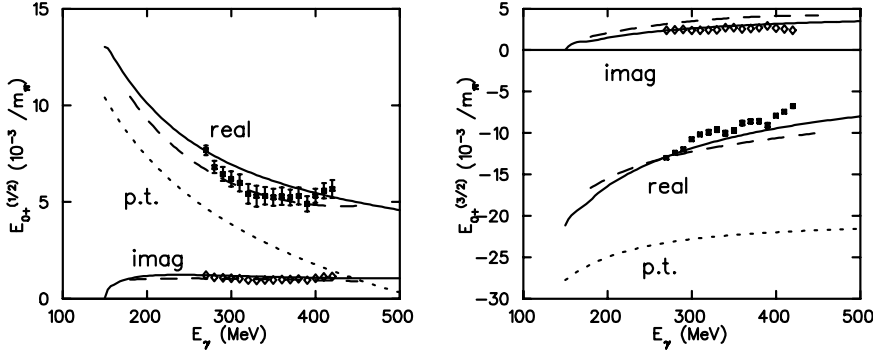


Figure 2. The real and imaginary parts and the pole term (p.t.) contributions of the amplitudes  $E_{0+}(1/2)$  and  $E_{0+}(3/2)$ . The results of our fit (solid lines) are compared with those from Ref. <sup>10</sup> (dashed lines). The data points are the result of our energy independent fit.

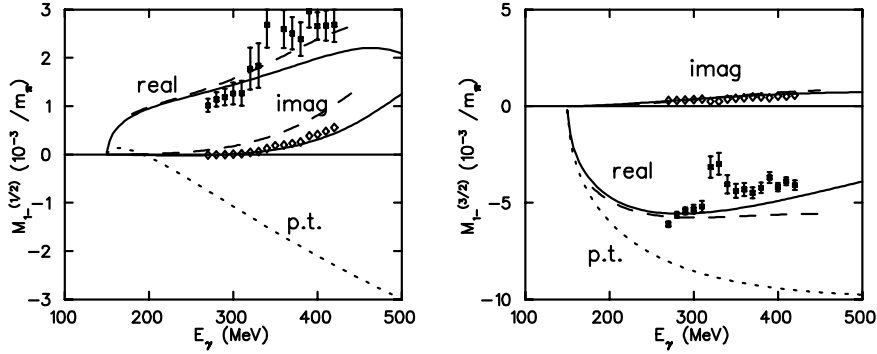


Figure 3. The real and imaginary parts and the pole term (p.t.) contributions of the amplitudes  $M_{1-}(1/2)$  and  $M_{1-}(3/2)$ . Symbols as in Fig. 2.

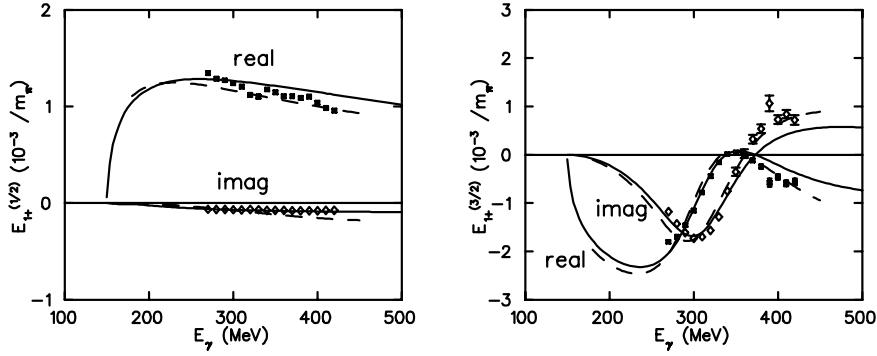


Figure 4. The real and imaginary parts of the amplitudes  $E_{1+}(1/2)$  and  $E_{1+}(3/2)$ . Symbols as in Fig. 2.

After appropriate simplifications, namely neglect of weakly coupling integral kernels and restriction to the partial waves of low angular momentum, the integral equations (8) can be solved in different ways. We based our analysis on the method of Omnès<sup>8</sup> because this method leads to a parametrization of the multipoles in a natural way and thus allows for analyzing experimental data. As an additional input, the solution of the integral equations requires the phases  $\phi_l^I(W)$  of the multipoles on the whole range of integration. According to the Fermi-Watson theorem, these phases are equal to the corresponding  $\pi N$  scattering phase shifts below  $2\pi$  threshold,  $\phi_l^I(W) = \delta_l^I(W)$ . Above  $2\pi$



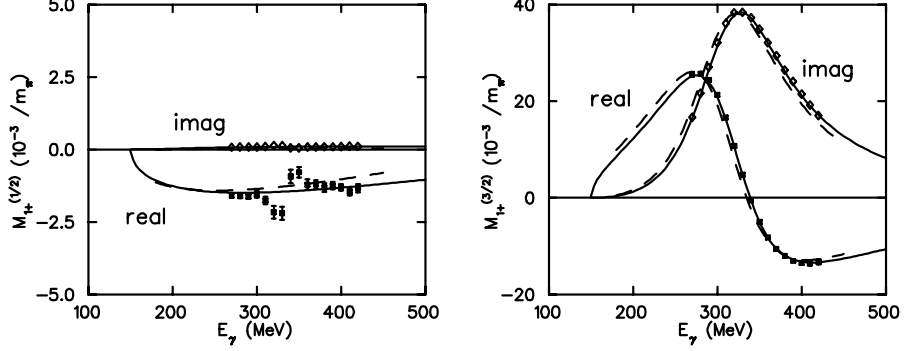


Figure 5. The real and imaginary parts of the amplitudes  $M_{1+}(1/2)$  and  $M_{1+}(3/2)$ . Symbols as in Fig. 2.

threshold, we use the ansatzes

$$\phi_l^I(W) = \arctan\left(\frac{1 - \eta_l^I(W) \cos 2\delta_l^I(W)}{\eta_l^I(W) \sin 2\delta_l^I(W)}\right). \quad (9)$$

for the  $S_{11}$ ,  $P_{11}$ ,  $P_{33}$ , and  $D_{13}$  waves, and

$$\phi_l^I(W) = \arctan\left(\frac{\eta_l^I(W) \sin 2\delta_l^I(W)}{1 + \eta_l^I(W) \cos 2\delta_l^I(W)}\right), \quad (10)$$

for the  $S_{31}$ ,  $P_{13}$ , and  $P_{31}$  waves. These ansatzes are each based on unitarity<sup>9</sup> and an additional assumption. They contain the scattering phase shifts  $\delta_l^I(W)$  and the inelasticity parameters  $\eta_l^I(W)$  of  $\pi N$  scattering. Both ansatzes give  $\phi_l^I(W) = \delta_l^I(W)$  below  $2\pi$  threshold. Since partial wave analyses of  $\pi N$  scattering are only available up to about  $W = 2$  GeV, we cut the integrals off at this energy to avoid the integration of unknown functions. Instead we represented the contributions of the imaginary parts at higher energies by  $t$ -channel exchange of vector mesons. The integral equations then take the form

$$\begin{aligned} M_l^I(W) &= M_l^{I,\text{pole}}(W) + \frac{1}{\pi} \int_{W_{\text{thr}}}^{\Lambda} \frac{h_l^{I*}(W') M_l^I(W') dW'}{W' - W - i\varepsilon} \\ &+ \frac{1}{\pi} \sum_{l', I'} \int_{W_{\text{thr}}}^{\Lambda} K_{ll'}^{II'}(W, W') h_{l'}^{I'*}(W') M_{l'}^{I'}(W') dW' + M_l^{I,V}(W), \end{aligned} \quad (11)$$

where  $\Lambda = 2$  GeV.

The solutions relevant for our case are the sum of a particular solution, which contains the inhomogeneities as driving terms, and a solution to the homogeneous equation multiplied by an arbitrary real coefficients  $c_l^f$ :

$$\mathcal{M}_l^I(W) = \mathcal{M}_l^{I,\text{part}}(W) + c_l^f \mathcal{M}_l^{I,\text{hom}}(W). \quad (12)$$

The coefficients  $c_l^f$  are the fitting parameters in our procedure. In addition, we varied the coupling constants of the  $\omega$  and the  $\rho$  meson. Since the addition of the homogeneous solution is only allowed for multipoles for which the phase is different from zero in the asymptotic limit, we decided to fit the parameters  $c_l^f$  only for the following multipoles:  $E_{0+}(0)$ ,  $E_{0+}(1/2)$ ,  $M_{1-}(0)$ ,  $M_{1-}(1/2)$ ,  $E_{1+}(3/2)$  and  $M_{1+}(3/2)$ . So we end up with a 10 parameter fit, the results of which are discussed in the next section.

### 3.2 Results

The fit to the benchmark data set leads to an overall  $\chi^2$  of 3.7 per data point. This high value is mainly due to the differential cross sections and target asymmetries of  $\pi^0$  production (see Table 4).

Table 4. The  $\chi^2$  per data point in our fit for the individual observables. It is seen that, except for the beam asymmetry  $\Sigma$ , the description of  $\pi^0$  production data is much poorer than that of  $\pi^+$  production data.

	$\pi^0 p$	$\pi^+ n$
$d\sigma/d\Omega$	7.4	2.8
$\Sigma$	1.2	1.6
$T$	5.2	2.9

The magnitudes of the vector meson coupling constants as determined by our fit differ somewhat from the values quoted in the literature. This can be attributed to the fact that the dispersion integrals up to 2 GeV already contain a certain fraction of the vector meson contributions (see Table 5).

Our results for the s- and p-wave multipoles are shown in Figs. 2 to 5. As the procedure presented by Inna Aznauryan<sup>10</sup> at this workshop is closely related to ours, her results are also shown for comparison. The real parts of the  $E_{0+}$  and  $M_{1-}$  multipoles differ significantly from the pole term contributions. In our approach, this difference, which in other approaches has to be provided by mechanisms like rescattering, is due to contributions from dispersion integrals.

Table 5. Comparison between the vector meson coupling constants resulting from our fit and values quoted in the literature.

	$g_\rho^V$	$g_\rho^T$	$g_\omega^V$	$g_\omega^T$
this work	4.85	15.69	6.78	-1.67
Ref. <sup>11</sup>	3.24	19.81	15.85	0
Ref. <sup>12</sup>	1.99	12.42	20.86	-3.41

#### 4 Analysis of Low-Energy Benchmark Data Using Fixed-t Dispersion Relations

[ I.G.Aznauryan ]

In this analysis the low-energy benchmark data are analyzed using fixed-t dispersion relations within the approach which is close to the approach developed in Refs. <sup>13,14,15,16</sup>. The real parts of the amplitudes are constructed through real parts of invariant amplitudes  $A_i^{(\pm,0)}(s,t)$ ,  $i = 1, 4$  (Ref. <sup>17</sup>), which are obtained using fixed-t dispersion relations:

$$\text{Re}A_i^{(\pm,0)}(s,t) = A_i^{Pole}(s,t) + \frac{P}{\pi} \int_{s_{thr}}^{s_{max}} \text{Im}A_i^{(\pm,0)}(s',t) \left( \frac{1}{s'-s} + \frac{\eta_i \eta^{(\pm,0)}}{s'-u} \right) ds', \quad (13)$$

with

$$A_i^{Pole}(s,t) = A_i^{Born}(s,t) + A_i^\omega(s,t) + A_i^\rho(s,t) \quad (14)$$

where  $\eta^{(+,0)} = -\eta^{(-)} = 1$ ,  $\eta_1 = \eta_2 = -\eta_3 = \eta_4 = 1$ .  $A_i^{Born}(s,t)$  are the contributions of the nucleon poles in the s- and u-channels and of the pion pole in the t-channel. In the dispersion relations<sup>13</sup>, the dispersion integrals are taken over resonance energy region up to  $s_{max} = (2 \text{ GeV})^2$ , and it is supposed that the integrals over higher energies can be approximated by the t-channel  $\omega$  and  $\rho$ -contributions:  $A_i^\omega(s,t)$ ,  $A_i^\rho(s,t)$ . These contributions are taken in the form presented in Ref. <sup>6</sup>. The integrals over resonance energy region are saturated by the resonances used in the VPI analysis of pion photoproduction data <sup>4</sup>. The coupling constants for all resonances, except  $P_{33}(1232)$ , are taken from this analysis. The resonance contributions are parametrized in the Breit-Wigner form according to Ref.<sup>18</sup>.

The multipole amplitudes  $M_{1+}^{3/2}$  and  $E_{1+}^{3/2}$  corresponding to the  $P_{33}(1232)$  resonance are parametrized using the approach developed in Refs. <sup>9,19</sup>. Ac-

$\text{Im}M_{1+}^{3/2}$	$52.458 \pm 0.002 \text{ mFm}$
$\text{Im}E_{1+}^{3/2}$	$-1.19 \pm 0.01 \text{ mFm}$
$E2/M1$	-0.023

Table 6. The amplitudes  $M_{1+}^{3/2}, E_{1+}^{3/2}$  at the resonance position.

	Present analysis	Ref. <sup>6</sup>	Ref. <sup>3</sup>	Ref. <sup>20</sup>
$g_{\omega}^V$	4	6.8	21	8-14
$g_{\omega}^T$	-24	-1.7	-12	0-(-14)
$g_{\rho}^V$	2.5	4.9	2	1.8-3.2
$g_{\rho}^T$	21	16	13	8-21

Table 7. The  $\omega NN$  and  $\rho NN$  coupling constants in comparison with results from other sources.

According to this approach the amplitudes  $M_{1+}^{3/2}, E_{1+}^{3/2}$  are the solutions of the singular integral equations which follow from dispersion relations for these amplitudes, and have the form:

$$M(s) = M_{part}^{Born}(s) + M_{part}^{\omega}(s) + c_M M^{hom}(s), \quad (15)$$

where  $M(s)$  denotes any of the amplitudes  $M_{1+}^{3/2}, E_{1+}^{3/2}$ .  $M_{part}^{Born}(s)$  and  $M_{part}^{\omega}(s)$  are the particular solutions of the integral equations generated by the Born and  $\omega$  contributions. Particular solutions have definite magnitudes fixed by these contributions.  $M^{hom}(s)$  is the solution of the homogeneous part of the integral equation; it has a certain energy dependence fixed by the integral equation and an arbitrary weight which was found by fitting the data.

In the  $P_{33}(1232)$  resonance region we have taken into account also the contributions of the non-resonant multipoles  $E_{0+}^{1/2}, E_{0+}^{(0)}, E_{0+}^{3/2}, M_{1-}^{1/2}, M_{1-}^{(0)}$  into  $\text{Im}A_i^{(\pm,0)}(s, t)$ . These multipole amplitudes were found by calculating their real parts from the dispersion relations<sup>13</sup>; then the imaginary parts of the multipole amplitudes at  $W < 1.3 \text{ GeV}$  were found using the Watson theorem. At higher energies the smooth cutoff of these contributions was made.

Our fitting parameters were:

(1) the constants  $c_M$  and  $c_E$  which correspond to the magnitudes of homogeneous solutions for  $M_{1+}^{3/2}, E_{1+}^{3/2}$  in Eq. 15 at the resonance position;

	$\sigma(\pi^+)$	$A(\pi^+)$	$T(\pi^+)$	$\sigma(\pi^0)$	$A(\pi^0)$	$T(\pi^0)$
$\chi^2/N$	922/317	440/253	245/107	2568/347	276/192	394/71

Table 8. The values of  $\chi^2$ .

(2) the coupling constants  $g_\omega^V$ ,  $g_\omega^T$ ,  $g_\rho^V$ ,  $g_\rho^T$  which describe the  $\omega$  and  $\rho$  contributions in Eq. 14.

(3) we have also included into the fitting procedure the coupling constants for the resonances  $S_{11}(1535)$ ,  $P_{11}(1430)$  and  $D_{13}(1520)$ , namely, the coupling constants for the multipoles  $E_{0+}^{1/2}$ ,  $E_{0+}^{(0)}$  of  $S_{11}(1535)$ , for the multipoles  $M_{1-}^{1/2}$ ,  $M_{1-}^{(0)}$  of  $P_{11}(1430)$ , and for the multipoles  $E_{2-}^{1/2}$ ,  $E_{2-}^{(0)}$ ,  $M_{2-}^{1/2}$ ,  $M_{2-}^{(0)}$  of  $D_{13}(1520)$ . A small variation of these coupling constants around the values obtained in the analysis of Ref. <sup>4</sup> was allowed.

The obtained results are presented in Tables 6-8.

## 5 The Effective Lagrangian Analysis of the Benchmark Dataset

[ R. M. Davidson ]

### 5.1 The Model

Details of the effective Lagrangian approach(ELA) to pion photoproduction may be found in Ref.<sup>21</sup>. Here I briefly summarize the main features of the model. The effective Lagrangian consists of the pseudovector (PV) nucleon Born terms,  $t$ -channel  $\omega$  and  $\rho$  exchange, and  $s$ - and  $u$ -channel  $\Delta(1232)$  exchanges. At the tree-level, the amplitude is gauge invariant, Lorentz invariant, crossing symmetric, and satisfies the LET's for these reactions to order  $m_\pi/M$ . However, the tree-level amplitude violates unitarity. To unitarize this amplitude, the tree-level multipoles,  $\mathcal{M}_l^T$ , are projected out and unitarized via a K-matrix approach;

$$\mathcal{M}_l = \mathcal{M}_l^T \cos \delta_l e^{i\delta_l}, \quad (16)$$

where  $\delta_l$  is the appropriate  $\pi N$  elastic scattering phase shifts. In practice, this is done only for the  $s$ - and  $p$ -wave multipoles. In order to keep multipoles of all  $l$  values, the unitarized multipoles are added to the tree-level CGLN  $\mathcal{F}$ 's<sup>22</sup> and the tree-level multipoles are subtracted. To give a simple example, if only  $E_{0+}$  is unitarized, then  $\mathcal{F}_1$  in this model is

$$\mathcal{F}_1 = \mathcal{F}_1^T + E_{0+}^T (\cos \delta_0 e^{i\delta_0} - 1), \quad (17)$$

where  $\mathcal{F}_1^T$  is the tree-level approximation to  $\mathcal{F}_1$ .

After unitarization, one is now ready to fix the parameters of the model. The  $\Delta$  mass,  $M_\Delta$ , and width  $\Gamma$  are determined by a fit to the  $P_{33}$  phase shift and are not varied in the photoproduction fit. The pion and nucleon masses are fixed at 139.6 and 938.9 MeV, respectively. Although one could look at the sensitivity of the photoproduction data to the pion-nucleon coupling constant, I keep the PV coupling constant,  $f$ , fixed at a value of 1.0. The  $\rho$  and  $\omega$  are taken to be degenerate with a mass of 770 MeV, and the  $V\pi\gamma$  ( $V = \rho$  or  $\omega$ ) coupling constants are taken from the known radiative decays  $V \rightarrow \pi\gamma$ . The Dirac and Pauli-like  $VNN$  coupling constants were allowed to vary in the fit. The remaining parameters of the model are related to the  $\Delta$  interactions. Of most interest are the two  $\gamma N\Delta$  coupling constants,  $g_1$  and  $g_2$ , which are related to M1 and E2 by

$$M1 = \frac{e}{12M} \left( \frac{k_\Delta}{M_\Delta M} \right)^{1/2} \left\{ g_1(3M_\Delta + M) - g_2 \frac{M_\Delta}{2M} (M_\Delta - M) \right\} ,$$

$$E2 = -\frac{e}{6M} \frac{k_\Delta}{(M_\Delta + M)} \left( \frac{k_\Delta M_\Delta}{M} \right)^{1/2} \left\{ g_1 - g_2 \frac{M_\Delta}{2M} \right\} ,$$

where  $k_\Delta = (M_\Delta^2 - M^2)/(2M_\Delta)$ . The remaining parameters are the off-shell parameters, X,Y,Z, associated with the  $\Delta$  transition vertices. For example, the  $\pi N\Delta$  Lagrangian is of the form

$$\mathcal{L} \sim \bar{\Delta}^\mu (g_{\mu\nu} + a\gamma_\mu\gamma_\nu) N \partial^\nu \pi + \text{h.c.} , \quad (18)$$

where  $a$  depends linearly on Z. Thus, the off-shell parameters essentially control the relative strength of the  $\gamma_\mu\gamma_\nu$  term compared to the  $g_{\mu\nu}$  term. It should be noted that when calculating matrix elements involving the off-shell parameters the pole in the  $\Delta$  propagator is canceled. Thus, the contributions involving the off-shell parameters appear as contact terms. As the off-shell parameters are fitted to the data, these contact terms can partially compensate for the lack of strong form factors which might arise, for example, from pionic dressing of the vertices.

## 5.2 Results and Discussion

The nine parameters of the model were fitted to the low-energy benchmark dataset consisting of 1287 data points. The total  $\chi^2$  was 5203 giving a  $\chi^2/df$  of 4.07. The breakdown of the  $\chi^2$  according to observable is given in Table 9. It is seen that the highest  $\chi^2/n$  are for  $d\sigma/d\Omega(\pi^0)$  and  $T(\pi^0)$ , which was true for the other analyses also. The best agreement was with the photon asymmetry,  $\Sigma$ , for both  $\pi^0$  and  $\pi^+$ .

As the  $\chi^2$  in this analysis is slightly larger than in the other analyses, it is useful to look at the  $\chi^2$  breakdown in energy bins. This is shown in Table 10, where  $[x, y)$  and  $[x, y]$  have their usual mathematical meaning. It is seen that the fit to the lowest energy bin is extremely poor. Most of the data in this energy interval are  $\pi^0$  differential cross section data, and a comparison of the fit with these data shows that the fit has too large of a forward-backward asymmetry as compared to the data. At these energies, this asymmetry is determined by the interference between the  $E_{0+}$  and the p-wave multipoles. A comparison of this multipole obtained in this fit with the same multipole obtained from fits that reproduce these low-energy data shows a significant difference.

Table 9.  $\chi^2$  for each observable fitted.

OBS	n	$\chi^2$	$\chi^2/n$
$d\sigma/d\Omega(\pi^+)$	317	988.4	3.1
$d\sigma/d\Omega(\pi^0)$	354	2804.0	7.9
$\Sigma(\pi^+)$	245	388.0	1.6
$\Sigma(\pi^0)$	192	258.1	1.3
$T(\pi^+)$	107	274.9	2.6
$T(\pi^0)$	72	489.6	6.8

Table 10.  $\chi^2$  as a function of energy bin fitted.

Interval	n	$\chi^2$	$\chi^2/n$
[180, 210)	64	747.7	11.7
[210, 240)	137	767.6	5.6
[240, 270)	208	803.6	3.9
[270, 300)	181	578.3	3.2
[300, 330)	191	516.8	2.7
[330, 390)	157	598.6	3.8
[360, 390)	120	265.5	2.2
[390, 420)	132	307.6	2.3
[420, 450)	97	615.4	6.3

At the BRAG workshop, we were able to understand this difference. As L. Tiator pointed out, at low-energies for  $\pi^0$  production, the coupling to the  $\pi^+n$  channel can be important and one must somehow account for processes

like

$$\gamma p \rightarrow n\pi^+ \rightarrow p\pi^0. \quad (19)$$

In dispersion relation models<sup>6,23</sup> and dynamical models<sup>2</sup>, this channel coupling is dynamically taken into account. In partial wave analyses<sup>4</sup>, the parametrization is flexible enough to account for this physics. In the isobar model<sup>3</sup>, this important physics was included in a semi-phenomenological manner. In the ELA, this channel coupling is only partially taken into account via the unitarization. However, dispersive corrections are not explicitly accounted for. It is implicitly assumed that the main effect of the dispersive corrections is to renormalize the parameters to their physical values. It is further assumed (or hoped) that any additional dispersive corrections can be accounted for by the contact terms coming from the off-shell parameters. Evidently, this is not the case over the entire fitted energy range. Thus, to improve the low-energy fit, without destroying the fit near the peak of the resonance, this additional physics would need to be added by hand to the ELA.

The parameters from the fit are shown in Table 11 along with representative parameters from Ref.<sup>21</sup>. The resulting resonance couplings are

$$\begin{aligned} M1 &= 286.2 \times 10^{-3} \text{GeV}^{-1/2} \\ E2 &= -7.21 \times 10^{-3} \text{GeV}^{-1/2} \\ \frac{E2}{M1} &= -2.55\%. \end{aligned} \quad (20)$$

Table 11. Parameters obtained in this fit (B.M.) compared with those obtained in <sup>21</sup>.

Par.	B.M.	DMW
$g_1$	5.06	$5.01 \pm 0.22$
$g_2$	4.72	$5.71 \pm 0.43$
Z	-0.25	$-0.30 \pm 0.12$
Y	1.65	$-0.38 \pm 0.66$
X	-5.74	$1.94 \pm 2.28$
$g_{\omega 1}$	-0.09	8
$g_{\omega 2}$	4.46	-8
$g_{\rho 1}$	1.51	2.66
$g_{\rho 2}$	3.66	16.2

The  $g_1$  coupling, which is mostly responsible for the  $M1$  strength, has not changed much compared to the earlier work.  $g_2$ , which determines the strength of  $E2$  has changed within the error bar. As a rule of thumb, the



smaller  $g_2$ , the larger in magnitude  $E2$ . The change in  $g_2$ , and hence  $E2$ , is probably due to the new high-precision  $\Sigma$  data<sup>24,25</sup>. The off-shell parameter  $Z$  has not changed much, but the other parameters have. This is partly due to the fact that the vector meson couplings were allowed to vary in this fit, but not in Ref.<sup>21</sup>. Since I did not do an error analysis for the BM fit, it is hard to say if the changes are significant. I do know that the vector meson couplings and off-shell parameters are highly correlated fit parameters. I should point out that the vector mesons are put in as point particles, i.e., no form factors. Thus, when I fit the vector meson coupling ‘constants’, I would expect them to decrease compared to their on-shell values. However, the results for the  $\omega$  seem unusual. The general conclusion at the BRAG workshop is that the  $\Delta$  region is not a good place to fit the vector meson couplings.

From a glance through the various multipole solutions, it seems to me that the model dependence is under good control in the  $\Delta$  region. One multipole that remains to be understood is the  $M_{1-}^{1/2}$ . Though all analyses pretty much agree on its numerical value, its physical interpretation is quite different in the various models. Is it a crossed- $\Delta$  effect or the tail of the Roper? In principle, the amplitude should be crossing symmetric, so if there is an s-channel  $\Delta$  exchange, there must be a u-channel  $\Delta$  exchange. In Ref.<sup>21</sup>, it was found that the  $M_{1-}^{1/2}$  multipole is largely insensitive to the off-shell parameters. Thus, these contributions cannot suppress the u-channel contribution in this multipole, and there is no room for a Roper contribution as large as in the isobar model. What is even more mysterious is that in Ref.<sup>21</sup> it was found that the Roper contribution enters with the opposite sign than the u-channel contribution (see Fig. 8 in<sup>21</sup>). Regarding the Roper contribution to this multipole, there are two clear possibilities. Either someone has made a mistake, or two different things are being compared. Certainly the latter is true to some extent. In Ref.<sup>21</sup>, both the s- and the u-channel Roper exchanges were included, whereas in the isobar model<sup>3</sup> only the s-channel contribution was included. Thus, it is possible that the s- and u-channel contributions destructively interfere in this multipole to produce the small effect found in<sup>21</sup>. I do not know the solution to this puzzle, but if dispersion relations are telling us there is a large crossing contribution to this multipole from the  $M_{1+}^{3/2}$ , then we must necessarily investigate this problem within the framework of a crossing symmetric model.

## 6 Multipole Analysis of the Benchmark Set Covering the First Resonance Region

[ A.S. Omelaenko ]

### 6.1 Introduction

A great deal of experimental data on the photoproduction of single pions is stored in compilations. There are problems connected with the normalization of some systematic measurements of the differential cross section. As a result, in multipole analyses, one has to reject or renormalize up to 10% of experimental points. This can throw some doubt on the extraction of delicate values, such as the E2/M1 ratio for the  $\Delta^+(1232)$ . This makes very interesting the comparison of analyses, based on different approaches, using the same test database for the most well investigated  $\gamma p \rightarrow p\pi^0(n\pi^+)$  reaction, with a strong accent on the modern data. Here we report on a fit to the low-energy dataset based on (a) the resonance model with polynomial parametrization of the background and (b) energy-independent fitting.

### 6.2 Formalism in the First Resonance Region

**Resonance Model.** Description of the  $P_{33} \pi N$  scattering amplitude is simple if it is taken to be purely elastic in the first resonance region. Similar to the form used in Ref.<sup>18</sup>, our multi-parameter model for single pion photoproduction is written as a sum of a background plus the  $\Delta^+(1232)$  resonance contribution. The real part of the background is given by the electric Born approximation which is completed in s-, p- and d-waves by a cubic polynomial of the form

$$\text{Re}M_{l\pm}^I(E_\gamma) = \sum_{i=1}^4 \text{Re}M_{l\pm}^I(E_\gamma^{(i)}) \prod_{\substack{j=1 \\ j \neq i}}^4 (E_\gamma - E_\gamma^{(j)}) / (E_\gamma^{(i)} - E_\gamma^{(j)}). \quad (21)$$

Here, depending on the laboratory photon energy  $E_\gamma$ , multipoles  $M_{l\pm}^I \equiv A_{l\pm}^I, B_{l\pm}^I$  are defined according to Ref.<sup>18</sup> with the isospin structure

$$\begin{aligned} A^{1/2} &= 1/3A_{\pi^0 p} + \sqrt{2}/3A_{\pi^+ n}, \\ A^{3/2} &= A_{\pi^0 p} - \sqrt{1/2}A_{\pi^+ n}. \end{aligned}$$

Index  $l$  is the orbital angular momentum, while + and - correspond to the total angular momentum  $j = l \pm 1/2$ . Imaginary parts of the background

multipoles are calculated according to Watson's theorem, using phase shifts from  $\pi N$  elastic scattering analyses:

$$\text{Im}M_{l\pm}^I = \text{Re}M_{l\pm}^I \tan(\delta_{2I,2(l\pm)}). \quad (22)$$

The resonant multipole amplitudes  $A_{1+}^{3/2}$  and  $B_{1+}^{3/2}$  have the following form

$$M_{1+}^{3/2}(E_\gamma) = M_{1+}^{3/2,R}(E_\gamma) + B_M(E_\gamma) \cos \delta_{33} e^{i\delta_{33}} \quad (23)$$

with the first term describing excitation of the resonance

$$M_{1+}^{3/2,R}(E_\gamma) = C_M \sqrt{\frac{k_0 q_0}{kq}} \frac{W_0 \sqrt{\Gamma \Gamma_\gamma}}{W_0^2 - W^2 - iW_0 \Gamma}, \quad (24)$$

with  $W$  and  $W_0$  being the total c.m. energy and its value at resonance, respectively,  $C_M$  being the resonance constant. The energy-dependent widths were parametrized by

$$\Gamma_\gamma(W) = \Gamma_0 \left( \frac{k}{k_0} \right)^2 \left( \frac{k_0^2 - X^2}{k^2 - X^2} \right)^2, \quad (25)$$

$$\Gamma(W) = \Gamma_0 \left( \frac{q}{q_0} \right)^2 \left( \frac{q_0^2 - X^2}{q^2 - X^2} \right)^2 \quad (26)$$

where  $k$  and  $q$  are the c.m. momenta of the photon and pion, respectively, and  $k_0$ ,  $q_0$  are the corresponding values at  $W_0$ . The second term in Eq. (23) corresponds to Noelle's unitary treatment of the background<sup>26</sup>. In our approach, the resonance term has a simplified form, not containing the elastic background phase shift  $\delta_B$ . However, this has practically no influence on the E2/M1 ratio, being quite independent of  $\delta_B$ <sup>27</sup>. The real background functions  $B_A(E_\gamma)$  and  $B_B(E_\gamma)$  are parametrized according to Eq. (21), each in terms of 4 knot values. The phase shift  $\delta_{33}$  is calculated as the phase of the Breit-Wigner form in Eq. (24):

$$\tan \delta_{33} = \frac{W_0 \Gamma(W)}{W_0^2 - W^2} \quad (27)$$

The resonance quantities  $C_A$ ,  $C_B$ ,  $W_0$ ,  $\Gamma_0$  were determined in the fit, along with the knot values of  $B_A$  and  $B_B$  and the real parts of the background multipoles:  $A_{0+}$ ,  $A_{1+}$ ,  $A_{1-}$ ,  $A_{2-}$ ,  $B_{1+}$ ,  $B_{2-}$  with  $I = 1/2$  and  $A_{0+}$ ,  $A_{1-}$  with  $I = 3/2$ . Inclusion of the d-wave multipoles is motivated by a possible influence of the second resonance region.

**Energy-Independent Version.** In order to fit narrow energy bins, we take the real parts of the abovementioned non-resonant multipoles as independent parameters. Eq. (22) is used to calculate imaginary parts, taking into

account the energy dependence of the phase shifts. To avoid calculational problems at the point where  $\delta_{33}$  passes through  $\pi/2$ , the resonant multipoles have been parametrized as

$$A_{1+}^{(3/2)} = A \exp(i\delta_{33}), \quad (28)$$

$$B_{1+}^{(3/2)} = B \exp(i\delta_{33}), \quad (29)$$

with  $A$  and  $B$  to be determined for each energy bin along with the real parts of all background multipoles.

### 6.3 Results from the Fits

**Resonance Model.** The whole energy interval was split into 3 subintervals, with knot values corresponding to the central values for energy-independent fits.

Fit 1	$180 \leq E_\gamma \leq 350$ MeV	$E_\gamma^{(1,2,3,4)} = 200, 250, 300, 350$ MeV
Fit 2	$250 \leq E_\gamma \leq 400$ MeV	$E_\gamma^{(1,2,3,4)} = 250, 300, 350, 400$ MeV
Fit 3	$300 \leq E_\gamma \leq 450$ MeV	$E_\gamma^{(1,2,3,4)} = 300, 350, 400, 450$ MeV

Fit	Data	$\chi^2$	N	$\chi^2/N$
Fit 1	Total	2026.5	930	2.18
	$\gamma p \rightarrow p\pi^0$	1332.4	460	2.90
	$\gamma p \rightarrow n\pi^+$	694.1	470	1.48
Fit 2	Total	1759.2	871	2.02
	$\gamma p \rightarrow p\pi^0$	1115.7	388	2.88
	$\gamma p \rightarrow n\pi^+$	643.5	483	1.33
Fit 3	Total	1259.7	697	1.81
	$\gamma p \rightarrow p\pi^0$	821.6	306	2.69
	$\gamma p \rightarrow n\pi^+$	438.1	391	1.12

Table 12. Fitting in the resonance model framework.

For each fit a total of 44 free parameters were searched (the parameter  $X$  turned out to be difficult to determine, and was fixed at Walker's value of 185 MeV). The statistical characteristics for all fits are given in Table 12, separately for the neutral and charged particle production. In Table 13, the contribution to  $\chi^2$  from individual experiments is given, as calculated from

Reaction	Observable	Label	N	$\chi^2/N$
$\gamma p \rightarrow p\pi^0$	$d\sigma/d\Omega$	FU96MA	45	2.2
	$d\sigma/d\Omega$	HA97MA	52	10.5
	$d\sigma/d\Omega$	BE97MA	77	1.4
	Sigma	BL92LE	16	3.3
	Sigma	BE97MA	77	0.8
	T	BO98BO	28	3.1
	T	BE83KH	26	3.6
$\gamma p \rightarrow n\pi^+$	$d\sigma/d\Omega$	FI72BO	32	0.9
	$d\sigma/d\Omega$	BR00MA	39	1.9
	$d\sigma/d\Omega$	BE00MA	140	1.7
	Sigma	BL00LE	57	1.7
	Sigma	BE00MA	140	0.9
	T	DU96BO	75	1.1

Table 13. Fits with the resonance model in the 250-400 MeV interval. See the database summary webpage to match abbreviations with full references.

Interval (MeV)	Mass (MeV)	Width (MeV)	E2/M1 (%)
180-350	$1232.6 \pm 1.0$	$121.1 \pm 6.0$	$-1.83 \pm 0.31$
250-400	$1231.7 \pm 0.7$	$118.4 \pm 3.9$	$-2.34 \pm 0.13$
300-450	$1230.6 \pm 0.8$	$116.5 \pm 3.9$	$-2.26 \pm 0.14$

Table 14. Resonance parameters for the  $\Delta(1232)$  from different energy intervals.

Fit 2. Finally, in Table 14, values for the resonance mass and width are given along with the corresponding value for the E2/M1 ratio.

**Energy-Independent Analysis.** Results from the resonance model fits were used as starting values for 10 parameters, which were determined by  $\chi^2$  minimization from the data contained in each 10 MeV bin. For all formally successful fits, the corresponding central values for photon energy, number of points (N) and  $\chi^2$  per degree of freedom is given in Table 15.

#### 6.4 Concluding Remarks

In the low-energy region, dominated by the first resonance, we find a rather good determination of the main s- and p-wave partial-wave amplitudes for pion photoproduction (on proton targets), taking into account d-wave corrections. Differences between the Fits 1-3 on overlapping energy intervals can be

$E_\gamma$ , MeV	$\chi^2$	N	$\chi^2/df$	$E_\gamma$ , MeV	$\chi^2$	N	$\chi^2/df$
210	10.1	18	1.27	330	100.6	51	2.45
220	18.6	43	0.56	340	20.0	49	0.51
230	23.8	22	1.99	350	118.3	74	1.85
240	52.9	58	1.10	360	6.3	32	0.29
260	112.3	71	1.84	370	28.9	42	0.90
270	33.3	36	1.28	380	93.1	46	2.59
280	171.5	69	2.91	390	16.7	42	0.52
290	72.9	51	1.78	400	86.8	56	1.89
300	81.3	80	1.16	410	16.7	34	0.70
310	121.8	59	2.49	420	67.2	50	1.68
320	96.8	69	1.64				

Table 15. Statistics of the energy-independent fits.

considered as some measure of the model error. In our analysis, a suspicious deviation in the energy dependence of the  $M_{1-}^{1/2}$  and  $M_{1+}^{1/2}$  was evident over the 380-420 MeV interval. Encouraging was the rather stable determination of the mass and width of the  $\Delta^+(1232)$  resonance and E2/M1 ratio within the framework of this model (Fits 2 and 3).

A comment of the chosen database is in order. Of the cross section data for neutral pion production, the set of HA97MA gives a  $\chi^2$  which is definitely too large. This is true in all of the fits. Problems seem concentrated mainly at the small and large angles. Unfortunately, the modern polarization data do not represent the complete set of single polarization observables. As a result, in some bins of the energy-independent fit, the experimental data were not sufficient for a successful minimization procedure, or yielded unreasonably low (less than 1) values for  $\chi^2/df$ . Further examination has shown that the abovementioned deviations in the energy behavior of the d-wave multipoles are due to the lack of reliable data as well. Precise new experiments would be extremely desirable.

## 7 SAID Multipole Analysis of the Benchmark Dataset

[ R.A. Arndt, I.I. Strakovsky, R.L. Workman ]

SAID fits were performed on both the low- and medium-energy datasets, using a phenomenological method described in Ref.<sup>4</sup>. Multipoles were parametrized

in the form

$$M = (A_{\text{phen}} + \text{Born})(1 + iT_{\pi N}) + B_{\text{phen}}T_{\pi N} \quad (30)$$

where  $A_{\text{phen}}$  and  $B_{\text{phen}}$  were constructed from polynomials in energy having the correct threshold behavior. An additional overall phase proportional to  $\text{Im}T_{\pi N} - T_{\pi N}^2$  was also allowed in order to allow deviations from the above form for waves strongly coupled to channels other than  $\pi N$ . This form clearly satisfies Watson's theorem, where valid, and allows a smooth departure as new channels become important. A real Born contribution is assumed for unsearched high partial-waves.

The overall fit to data is summarized in the Table below. While the fit to most quantities is about 2 per data point, there are clear exceptions. Our fit to the neutral-pion differential cross section and target polarization is significantly worse in the low-energy region. If  $\chi^2$  is calculated for the region between 450-1200 MeV a fairly uniform fit emerges, with all data types fitted equally well.

Observable	Low-Energy Fit (180-450)MeV	Medium-Energy Fit (180-1200)MeV	Medium-Energy Fit (450-1200) MeV
$\sigma(\theta)_{\pi^0 p}$	4.69	3.14	1.80
$\Sigma(\theta)_{\pi^0 p}$	1.24	2.05	2.32
$T(\theta)_{\pi^0 p}$	4.49	2.84	1.89
$\sigma(\theta)_{\pi^+ n}$	2.12	2.55	2.08
$\Sigma(\theta)_{\pi^+ n}$	1.46	1.81	2.36
$T(\theta)_{\pi^+ n}$	2.92	2.25	1.83

Table 16. Comparison of the low- and medium-energy fits in terms of  $\chi^2$ .

The poor fit to neutral-pion differential cross sections can be traced to the Haerter data from Mainz (Ph.D. Thesis, unpublished - see the database description on the BRAG webpage). This set contributed a  $\chi^2/\text{datum}$  of 10, the remaining data again having an overall  $\chi^2$  per data point of about 2.

Why the fit to target polarization should be poor is harder to determine. In the low-energy region, the benchmark dataset has taken target-polarization data from Kharkov and Bonn. Of these, the fit to Kharkov data is particularly bad. Our fit to the Bonn data is reasonable apart from the lowest-energy (and perhaps also the highest energy) set.

## 8 Conclusions and Future Projects

### 8.1 Database Issues

As this exercise was motivated by an earlier study of the E2/M1 ratio, and its database dependence, we should (at least) expect to verify the relative model-independence of this quantity (when a standard dataset is selected). This point was discussed by Davidson<sup>28</sup> in his contribution to NSTAR2001. From the combined set of benchmark fits, the E2/M1 ratio was found to be  $-2.38 \pm 0.27\%$ . Here the important quantity is the error, since a change in the fitted dataset could shift the central value.

Qualitative features of the fit to data were reasonably similar in the low-energy region. There was general agreement that the differential cross section and target polarization were badly fitted in the neutral-pion channel. In all cases, the thesis data of Haerter were identified as problematic for the differential cross section. [These data can be abandoned, as a new Mainz measurement<sup>29</sup> of the cross section and photon asymmetry for neutral-pion photoproduction has been analyzed and is nearing publication. This new set covers the full angular range and a wide range of energies.]

Unfortunately, such a simple solution was not evident for the target polarization. The fit to both the Bonn and Kharkov data is poor, with some sets suggesting a different shape. In this case, the general *disagreement* should motivate a re-measurement of this quantity, hopefully with better precision. A confirmation of the shape suggested by these data would be very difficult to accommodate.

### 8.2 Model Dependence

One ingredient common to all analyses is the Born contribution, usually augmented with vector-meson exchange diagrams. While it is tempting to determine an optimal set of vector meson couplings, over the fitted energy range, our study has shown this to be a very unstable procedure, when fits are restricted to the low-energy database.

The  $M_{1-}^{1/2}$  multipole, and its low-energy behavior, provides an interesting example of the model dependence encountered when one tries to decompose a partial-wave into its underlying ingredients. Hanstein has noted that, in his dispersion integral, the coupling  $M_{1+}^{3/2} \rightarrow M_{1-}^{1/2}$  exceeds  $M_{1-}^{1/2} \rightarrow M_{1-}^{1/2}$ . In the study of Davidson, this is accounted for by a u-channel  $\Delta$  exchange, a contribution absent in many isobar-model approaches. As a result, the Roper resonance contribution depends strongly on the set of approximations defining a fit.



### 8.3 Further Comparisons

One unique feature of this study was the construction of a site<sup>1</sup> containing, in one place, both the database and the multipole fits. This facility was built into the SAID site<sup>4</sup>, thus allowing a wide range of comparisons. Users can compare fits to observables (in both the benchmark and full database), the resulting multipoles, and search for regions of maximal agreement or disagreement.

### 8.4 Extensions of this Study

Having the present set of fits as a guide, it would be useful to repeat this study over a more carefully chosen database - containing, in some way, the effects of systematic errors. A second project of interest would be the extension to electroproduction, with the goal of understanding the model dependence seen in the extracted  $E_{1+}/M_{1+}$  and  $S_{1+}/M_{1+}$  ratios as a function of  $Q^2$ .

## References

1. The BRAG website (<http://cnr2.kent.edu/~manley/benchmark.html>) contains a detailed list of included data and the resulting fits.
2. S.S. Kamalov and S.N. Yang, Phys. Rev. Lett. **83**, 4494 (1999); S.N. Yang, J. Phys. G **11**, L205 (1985).
3. D. Drechsel, O. Hanstein, S.S. Kamalov and L. Tiator, Nucl. Phys. **A645**, 145 (1999).
4. R.A. Arndt, I.I. Strakovsky and R.L. Workman, Phys. Rev. C **53**, 430 (1996); most recent results are available at <http://gwdac.phys.gwu.edu>.
5. J. M. Laget, Phys. Rep. **69**, 1 (1981).
6. O. Hanstein, D. Drechsel and L. Tiator, Nucl. Phys. A **632**, 561 (1998).
7. J. S. Ball, Phys. Rev. **124**, 2014 (1961).
8. R. Omnès, Nuovo Cimento A **8**, 316 (1958).
9. D. Schwela und R. Weizel, Z. Phys. **221**, 71 (1969).
10. contribution of I. Aznauryan, described in Section 4.
11. R. Machleidt et al., Phys. Repts. **149**, 1 (1987).
12. P. Mergell, diploma thesis, Mainz (1995), and P. Mergell, U.-G. Meissner and D. Drechsel, NPA **596**, 367 (1996).
13. R.C.E. Devenish, D.H. Lith, Phys. Rev. D **5**, 47 (1972).
14. R.C.E. Devenish, D.H. Lith, Nucl. Phys. B **43**, 228 (1972).
15. R.C.E. Devenish, D.H. Lith, Nucl. Phys. B **93**, 109 (1975).
16. I.G. Aznauryan, S.G. Stepanyan, Phys. Rev. D **59**, 1(54009) (1999).
17. G.F. Chew et al, Phys. Rev. **106**, 1345 (1957)
18. R.L. Walker, Phys. Rev. **182**, 1729 (1969).

19. D. Schwela, H. Rolnik, R. Weizel, W. Korth, Z. Phys. **202**, 452 (1967).
20. O. Dumbrajs, R. Koch, P. Pilkuhn et al, Nucl. Phys. **B216**, 277 (1983).
21. R.M. Davidson, N.C. Mukhopadhyay and R.S. Wittman, Phys. Rev. D **43**, 71 (1991).
22. G.F. Chew, M.L. Goldberger, F.E. Low, and Y. Nambu, Phys. Rev. **106**, 1345 (1957).
23. I.G. Aznauryan, Phys. Rev. D **57**, 2727 (1998).
24. G. Blanpied *et al.*, Phys. Rev. Lett. **69**, 1880 (1992); *ibid*, **79**, 4337 (1997).
25. R. Beck *et al.*, Phys. Rev. Lett. **78**, 606 (1997); R. Beck and H. P. Krahn, *ibid*, **79**, 4510 (1997).
26. P. Noelle, Prog. Theor. Phys. **60**, 778 (1978).
27. A.S. Omelaenko and P.V. Sorokin, Sov. J. Nucl. Phys. **38**, 398 (1983); P. Christillin and G. Dillon, J. Phys. G **15**, 967 (1989).
28. R.M. Davidson, contribution to the Workshop on the Physics of Excited Nucleons (NSTAR 2001), Mainz, Germany, 7-10 March 2001.
29. R. Leukel, Ph.D. Thesis, Mainz 2001.